Supplementary Material For:

Molecular Engineering guided Dielectric Resonance Tuning in Derived Carbon Materials

Jiaoyan Shi,[1] Qiu Zhuang,[2] Lipeng Wu,[1,2] Ronghui Guo[1], Ling Huang,[1] Weijin Li,[3] Fan Wu, [1,*] Aming Xie[1,*]

[1] School of Mechanical Engineering, Nanjing University of Science & Technology, Nanjing 210094, China

[2] School of Chemistry and Chemical Engineering, Nanjing University of Science & Technology, Nanjing 210094, China

[3]School of Materials Science and Engineering, Nanjing University of Science & Technology, Nanjing 210094, China

*Corresponding Authors: wufan@njust.edu.cn (Fan Wu) and xieaming@njust.edu.cn (Aming Xie)

Tel: +86 152 5099 0521

Supplementary Material

Contents

1. Instruments and characterization

We observed the detailed morphology with scanning electron microscope(SEM, S4800, Hitachi) and high-resolution transmission electron microscope (HR-TEM, Tecnai G2 F20, FEI) which were equipped with an energy dispersive spectrometer(EDS). Data for structural analysis is measured by Fourier Transform Infrared spectrometer (FT-IR, Nicolet iS10, Thermal Fisher Scientific, USA). Thermogravimetry (TG, SDT Q600, TA) was adopted for the investigation of thermostability and X-ray photoelectron spectroscopy (XPS) was analyzed by an apparatus (ESCALAB 250Xi, Thermo Fisher Scientific) under inert gas. Samples for the electromagnetic property test were prepared via the mixture with wax and pressed into cylindrical specimens which would not affect the microstructure at the macron scale. Electrical conductivity was obtained from a Four-Point Probe Instrument (SZT-C, Suzhou Jingge Electronic). The vector network analyzer (VNA, N5242A PNA-X, Agilent) was employed for complex permittivity(ε_r) and complex permeability(μ_r).

2. Supplementary Figures

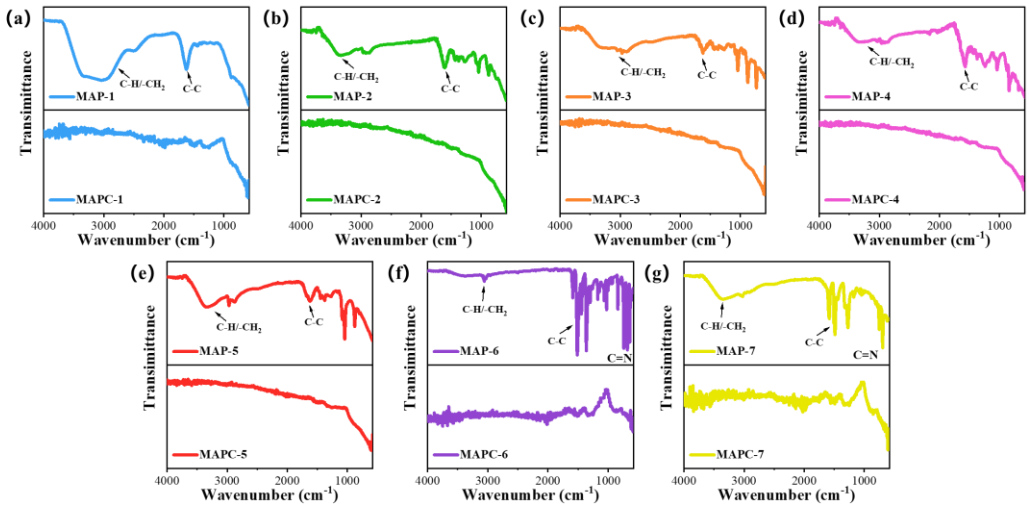

Figure S1 FTIR spectra of MAPs and MAPCs. The broad peak around 3200 cm^{-1} and a sharp peak around 1600 cm^{-1} are corresponding to stretching vibration of C-H, -CH_2, and C=C bonds. The peaks located in 1020-1360 cm^{-1} represent the C=N bonds in MAP-6 and MAP-7.

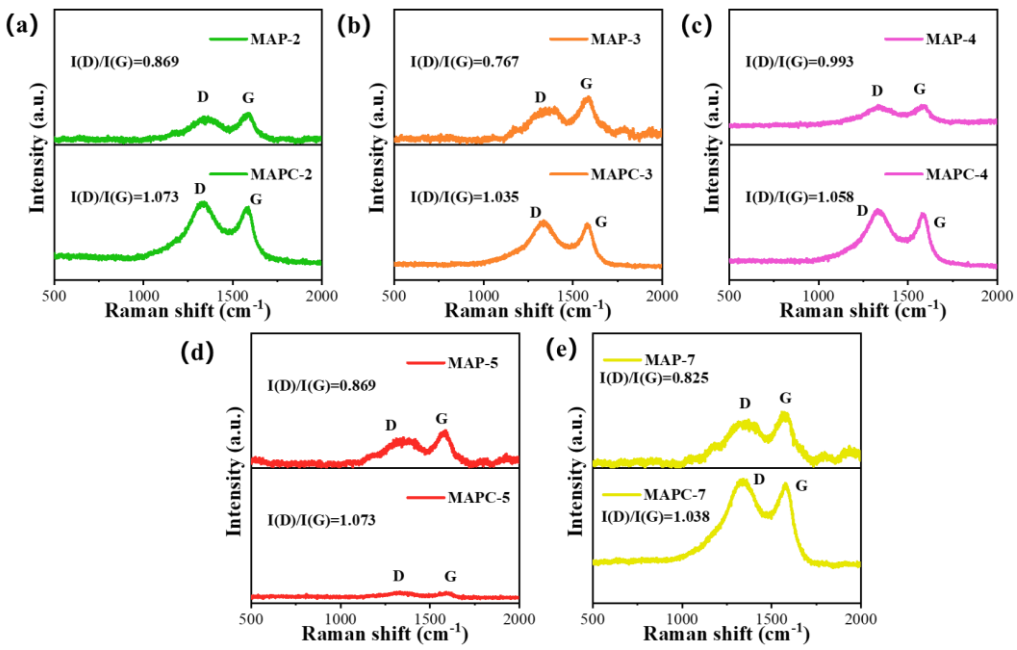

Figure S2 Raman spectra of MAPs and MAPCs. In MAPCs, the D band and G band signals are stronger than the D band and G band signals in MAPs, suggesting the existence of high conjugate structures in the precursors derived carbon materials.

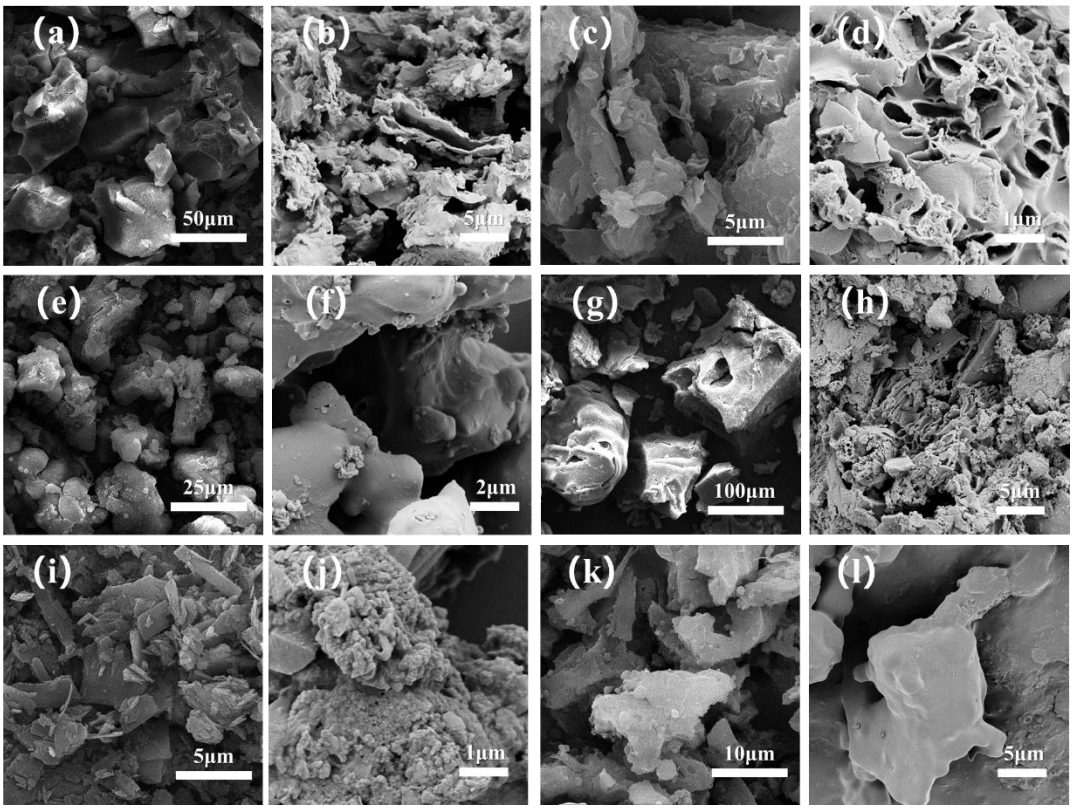

Figure S3 SEM images of MAPs and MAPCs; (a) MAP-1; (b) MAPC-1; (c) MAP-2; (d) MAPC-2; (e) MAP-3; (f) MAPC-3; (g) MAP-4; (h) MAPC-4; (i) MAP-6; (j) MAPC-6; (k) MAP-7; (l) MAPC-7. MAPs appear as bulk solid, while MAPCs demonstrate a foamy structure.

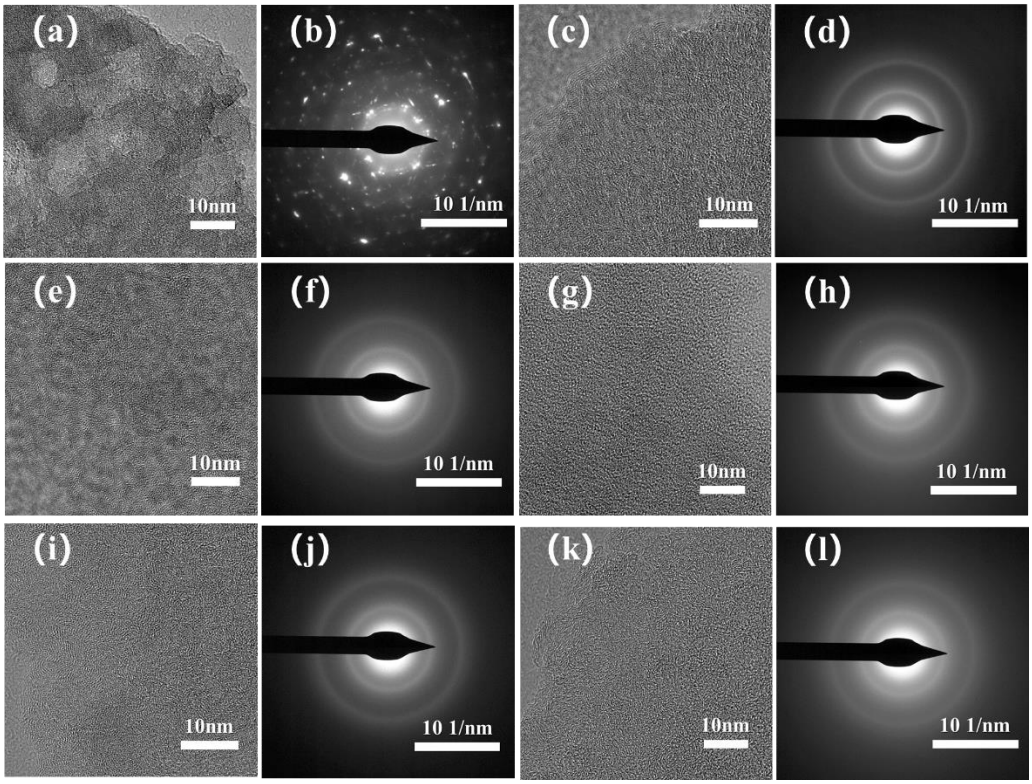

Figure S4 Carbon patterns and SAED of MAPCs; (a-b)MAPC-1; (c-d)MAPC-2; (e-f) MAPC-3; (g-h) MAPC-4; (i-j) MAPC-6;(k-l) MAPC-7. Some bright dots, assigning to the residual aluminum oxides, are observed in the HR-TEM images and unable to be removed by multi-washed (Figure S4b), which are further proved to be no contribution to the dielectric resonance of MAPCs.

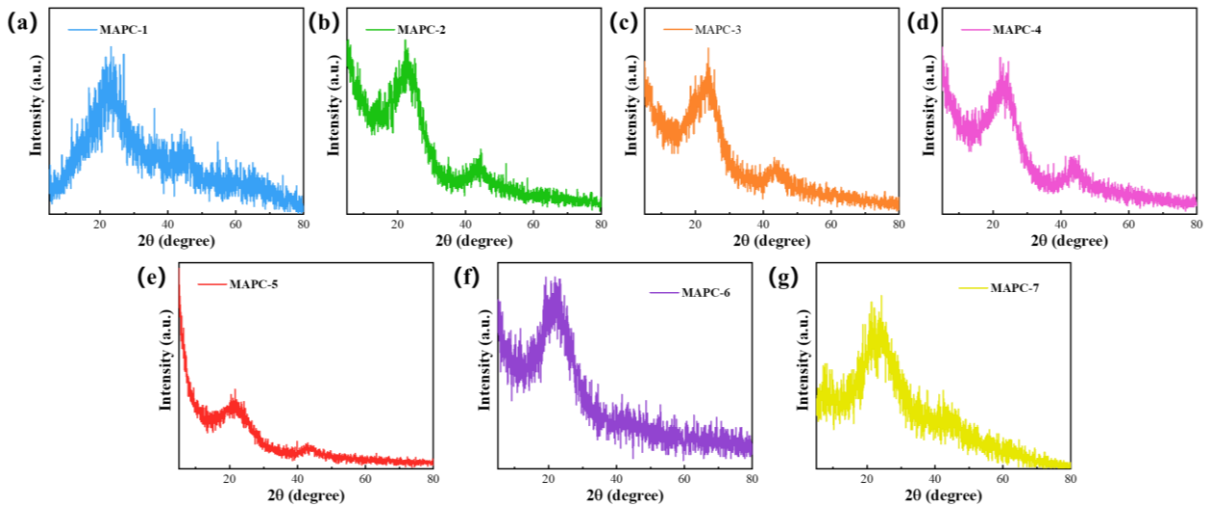

Figure S5 XRD patterns of MAPCs. The two broad peaks at 26.6 and 44.6 degree are agreeing well with the (100) and (110) lattice planes of graphite, suggesting a high degree of graphitization for MAPCs.

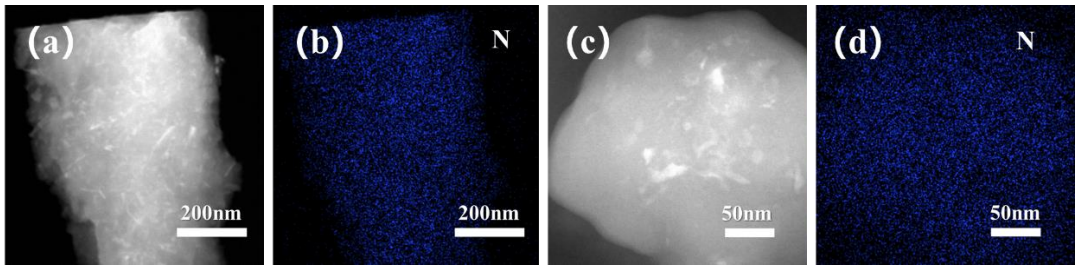

Figure S6 Elemental mapping of (a-b) MAPC-6 and (c-d) MAPC-7. The N element is homogeneously distributed in MAPC-6 and MAPC-7, suggesting the successful doping of the N-element into MAPCs.

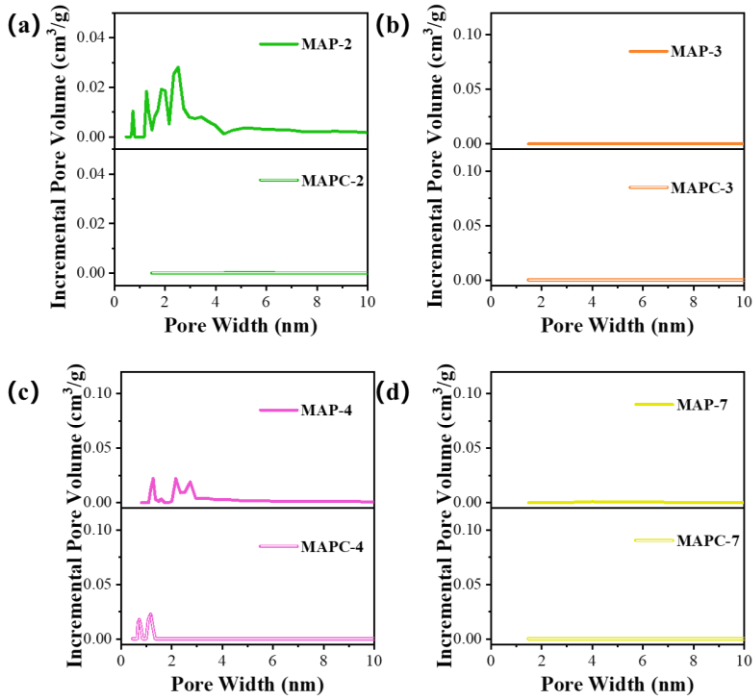

Figure S7 Pore distribution of (a)MAP-4 and MAPC-4, (b)MAP-7 and MAPC-7. MAPC-2 and MAPC-4 demonstrate a decreased specific surface area and pore size after the pyrolytic procedure. The MAPC-3 and MAPC-7 have no changed specific area and pore sizes compared to their pristine MAP-3 and MAP-7, respectively.

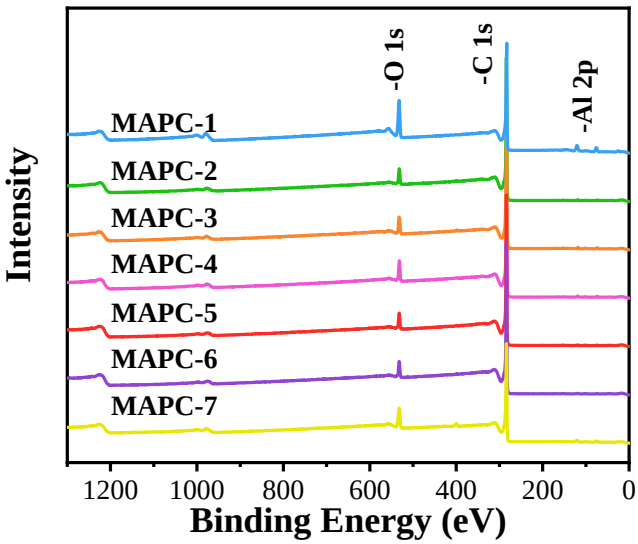

Figure S8 XPS survey. The residual aluminum element in MAPC-1 is determined by the full XPS spectrum (Figure S8), further indicating the existence of aluminum oxides. Apart from MAPC-1, no aluminum element can be distinguished from other MAPCs.

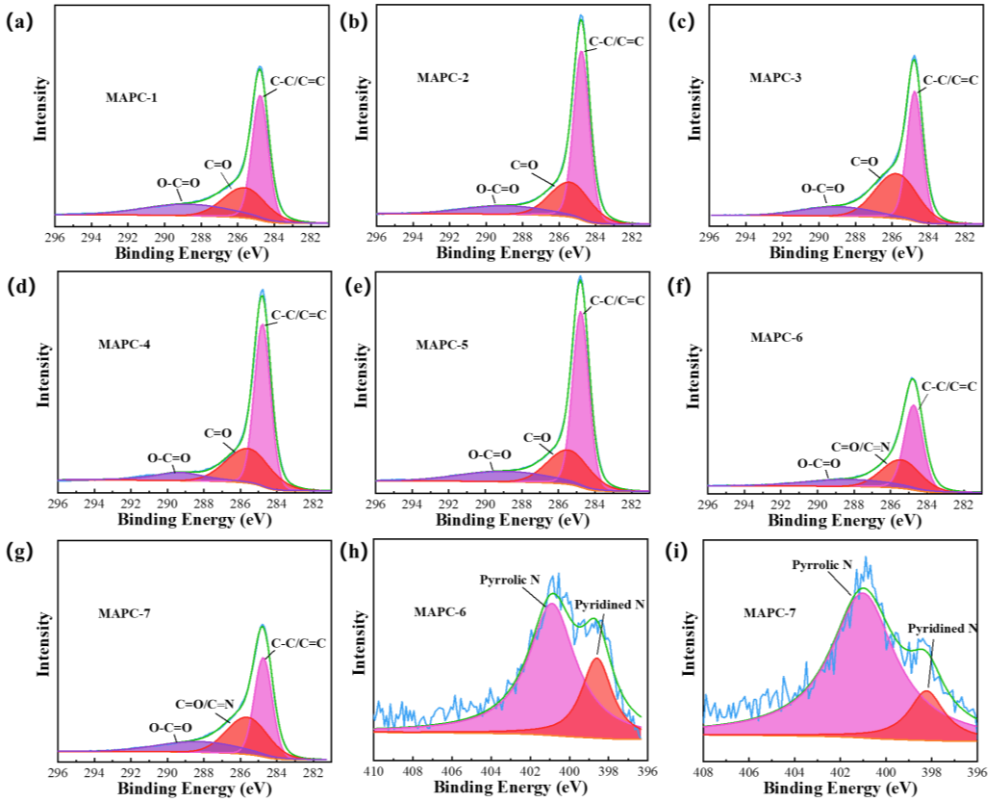

Figure S9 C 1s and N 1s spectra of MAPCs. The C1s spectra of MAPCs mainly show three peaks located at 284.8, 285.7, and 288.9 eV, attributing to C-C/C=C, C=O/C=N, and O-C=O bonds, respectively. These results suggest that the MAPCs 1-5 show the same composition. It is found two main peaks at 398.6 eV and 400.9 eV in N 1s spectra, which correspond to the pyrrolic N bond and pyridine N.

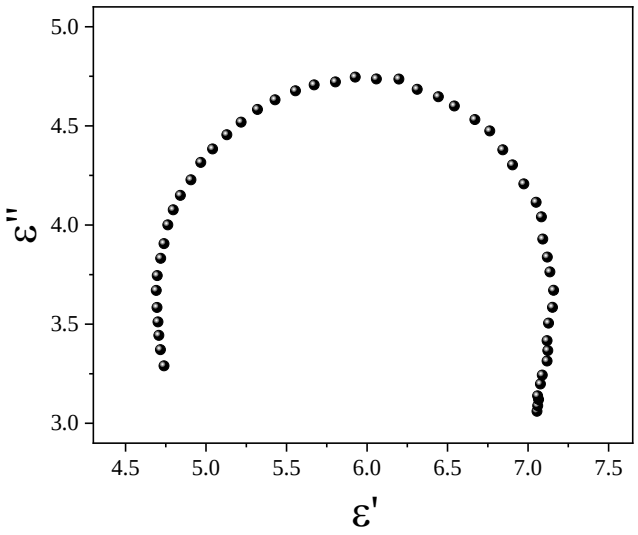

Figure S10 Cole-cole plot of MAPC-6 with a 10 wt% filler loading ratio.

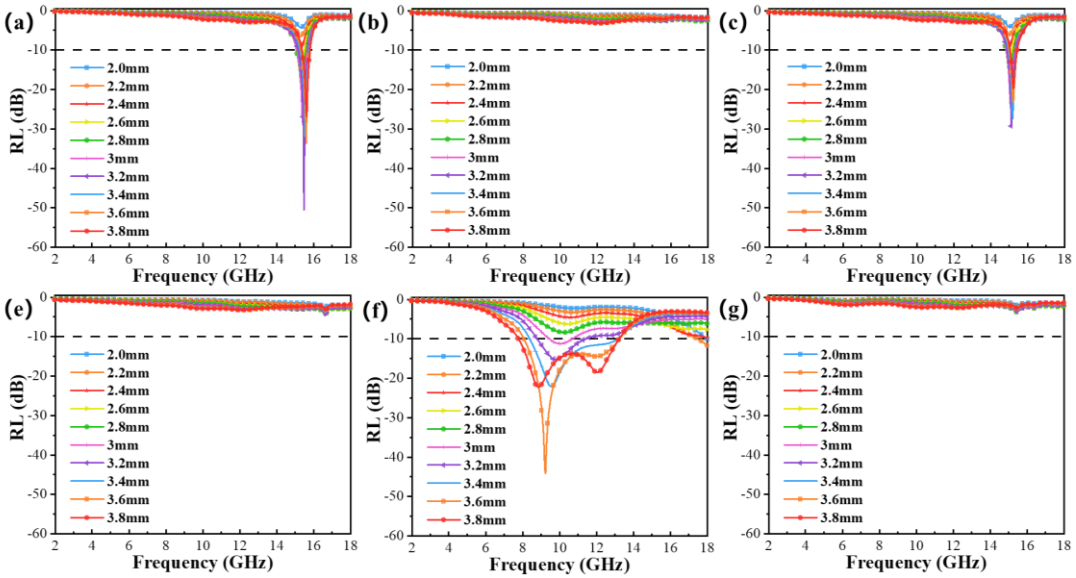

Figure S11 RL curves of MAPCs with a 5 wt% filler loading ratio. (a)MAPC-1; (b)MAPC-2; (c)MAPC-3; (d)MAPC-5; (e)MAPC-6; (f)MAPC-7. The decrease of filler loading ratio has no positive effect on the EMA performance of MAPCs.

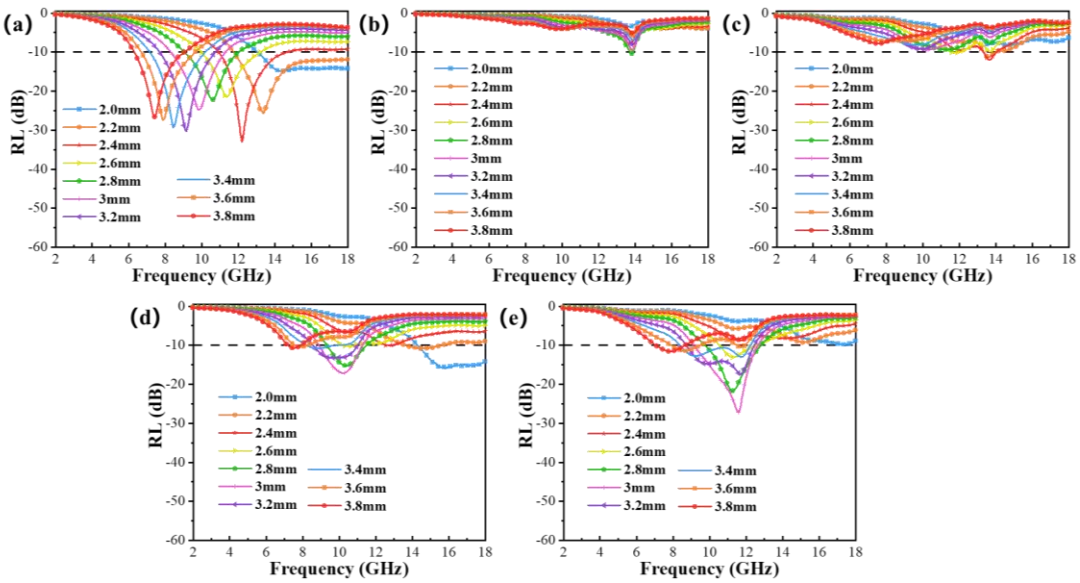

Figure S12 RL curves of MAPCs with a 15 wt% filler loading ratio. (a)MAPC-1; (b)MAPC-2; (c)MAPC-3; (d)MAPC-5; (e) MAPC-7. The increase of filler loading ratio has no positive effect on the EMA performance of MAPCs.

3. Supplementary Table

Compared to the electromagnetic wave absorbers, MAPC-6 could be the most promising candidate for the new generation of lightweight and high-performance EMA material due to its wide absorption bandwidth, low filler loading ratio, and adjustable absorption frequency.

Material	*EAB(GHz)*	*Width(mm)*	*Reference*
Co/NC/Mo$_x$C/NC	4.88	1.5	[1]
MnO/Ni	6.5	2.9	[2]
BCN nanosheet	4.16	1.4	[3]
CNTs/PyC HMs	4	2.3	[4]
NPC	5.7	2	[5]
MEHs	6.6	2.3	[6]
MHPFs	6.2	2	[7]
Cu/NC@Co/NC	5.19	2.5	[8]
CBC/CCW	6.28	2.5	[9]

4. Reference

[1] Y. Ge, G.I.N. Waterhouse, J. Sui, Z. Zhang and L. Yu, *Synth. Met.*, 2022, **287**, 117052.

[2] Y. Liu, Z. Zeng, S. Zheng, J. Qiao, W. Liu, L. Wu and J. Liu, *Composites, Part B.*, 2022, 109800.

[3] P. Mou, J. Zhao, G. Wang, S. Shi, G. Wan, M. Zhou, Z. Deng, S. Teng and G. Wang, *Chem. Eng. J.*, 2022, 135285.

[4] L. Kong, S. Luo, G. Zhang, H. Xu, T. Wang, J. Huang and X. Fan, *Carbon*. 2022, **61(7)**, 2799-2808.

[5] W. Yang, L. Yan, B. Jiang, P. Wang, Z. Li, C. Wang, H. Bai, C. Zhang and Y. Li, *Ind. Eng. Chem. Res.*, 2022.

[6] X. Lu, X. Li, W. Zhu and H. Xu, *Carbon*, 2022,**191**, 600-609.

[7] F. Wu, K. Yang, Q. Li, T. Shah, M. Ahmad, Q. Zhang and B. Zhang. *Carbon*, 2021, **173**, 918-931.

[8] H. Zhu, Q. Jiao, R. Fu, P. Su, C. Yang, C. Feng, H. Li, D. Shi and Y. Zhao, *J. Colloid Interface Sci.*, 2022, **613**, 182-193.

[9] S. Yin, Y. Huang, C. Deng, Y. Jiao, W. Wu, F. Seidi and H. Xiao, *Compos. Sci. Technol.*, 2022, **218**, 109184.